Cellular Uptake and Fate of PEGylated Gold Nanoparticles Is Dependent on Both Cell-Penetration Peptides and Particle Size

Eunkeu Oh,*,† James B. Delehanty,‡ Kim E. Sapsford,⊥ Kimihiro Susumu,† Ramasis Goswami,§ Juan B. Blanco-Canosa,¶ Philip E. Dawson,¶ Jessica Granek,⊥ Megan Shoff,⊥ Qin Zhang,⊥ Peter L. Goering,⊥ Alan Huston,† and Igor L. Medintz*,‡

†Optical Sciences Division, Code 5611, ‡Center for Bio/Molecular Science and Engineering, Code 6900, and §The Nanoscience Institute, Code 1100, U.S. Naval Research Laboratory, Washington, D.C. 20375, United States, ⊥Division of Biology, Office of Science and Engineering Laboratories, U.S. Food and Drug Administration, Silver Spring, Maryland 20993, United States, and ¶Departments of Cell Biology & Chemistry, The Scripps Research Institute, La Jolla, California 92037, United States

ABSTRACT Numerous studies have examined how the cellular delivery of gold nanoparticles (AuNPs) is influenced by different physical and chemical characteristics; however, the complex relationship between AuNP size, uptake efficiency and intracellular localization remains only partially understood. Here we examine the cellular uptake of a series of AuNPs ranging in diameter from 2.4 to 89 nm that are synthesized and made soluble with poly(ethylene glycol)-functionalized dithiolane ligands terminating in either carboxyl or methoxy groups and covalently conjugated to cell penetrating peptides. Following synthesis, extensive physical characterization of the AuNPs was performed with UV–vis absorption, gel electrophoresis, zeta potential, dynamic light scattering, and high resolution transmission electron microscopy. Uptake efficiency and intracellular localization of the AuNP–peptide conjugates in a model COS-1 cell line were probed with a combination of silver staining, fluorescent counterstaining, and dual mode fluorescence coupled to nonfluorescent scattering. Our findings show that AuNP cellular uptake is directly dependent on the surface display of the cell-penetrating peptide and that the ultimate intracellular destination is further determined by AuNP diameter. The smallest 2.4 nm AuNPs were found to localize in the nucleus, while intermediate 5.5 and 8.2 nm particles were partially delivered into the cytoplasm, showing a primarily perinuclear fate along with a portion of the nanoparticles appearing to remain at the membrane. The 16 nm and larger AuNPs did not enter the cells and were located at the cellular periphery. A preliminary assessment of cytotoxicity demonstrated minimal effects on cellular viability following peptide-mediated uptake.

KEYWORDS: gold nanoparticle · cell-penetrating peptide · cellular uptake · cytotoxicity · PEG · surface charge · endotoxin · dual mode fluorescence · silver staining

In recent years there has been growing interest in utilizing gold nanoparticles (AuNPs) for cellular applications including biomedical imaging, clinical diagnostics, and even therapeutics.[1−8] AuNPs are particularly useful for these applications, as they can function as contrast agents in optical imaging,[9] sensitizers for Raman scattering-based diagnostic probes,[7] and as vectors for photothermal therapy.[6] AuNP versatility arises from their inherent size and shape dependent optical properties which can be optimized to enhance the scattering and absorption cross sections within a particular application.[6] To reach their full potential in cellular applications, robust methods must be developed to allow for the controlled uptake of AuNPs into cells and for their localization to the cytosol or to other specific subcellular locations (*e.g.*, organelles) in a relatively benign manner. This requires the AuNPs to be functionalized with engineered coatings to promote hydrophilicity and biocompatibility along with specific targeting molecules to facilitate their cellular uptake and targeted delivery. However, the different combinations of particle shape, size, and surface coatings, along with further biofunctionalization usually present in these materials, result in the AuNPs displaying very complex physicochemical properties which significantly impact cellular uptake.

Numerous studies have examined cellular uptake of AuNPs to probe the underlying AuNP–cell interactions arising from their physicochemical characteristics.[10−21] Results have confirmed that size[11,14] and shape (for example: sphere,[11,14] rod,[17] shell,[15] cage,[6,11] and urchin[13]) of the AuNPs all alter the level of cellular uptake. In addition, surface chemistries, including charge,[10] ligand type, such as charged or neutral poly(ethylene glycol) (PEG),[6,10,11] and ligand morphology,[21] as well as conjugation to myriad biomolecules including oligonucleotides,[18] the tripeptide glutathione,[12] cell-penetrating peptides (CPPs),[16,19] nuclear localization signal (NLS) peptides,[19] and proteins[6,11,14,18] all dramatically influence uptake. Some underlying

* Address correspondence to Eunkeuoh@ccs.nrl.navy.mil, Igor.Medintz@nrl.navy.mil.

Received for review May 3, 2011 and accepted July 1, 2011.

Published online July 20, 2011
10.1021/nn201624c

relationships have begun to emerge from these studies indicating that uptake is most probably size-dependent.[11,22,23] Cellular response also appears to be size dependent,[14,23] and efficient AuNP uptake can be facilitated by a surface display of biomolecular mediators such as CPPs.[11,16,20,22,23] Concomitant with this, a lot of conflicting data has also arisen, especially concerning the upper size limit of AuNPs that can undergo cellular delivery along with effects of surface charge and ligand character.[10,11,14,20,22−24]Clearly, a full understanding of the underlying processes, which may ultimately lead to a highly desired predictive capability, requires a systematic and exhaustive analysis of all relevant parameters and indeed this challenge has already been put forth.[20,23] This understanding will also contribute to designing improved NP materials.

In this report, we synthesize a series of AuNPs ranging in size from 2.4 to 89 nm. These were synthesized and made biocompatible with PEG−functionalized dithiolane ligands that terminate in either a methoxy or carboxy group; the latter acting as a chemical handle for covalent modification to CPP. Following extensive characterization, a range of concentrations of the AuNP−CPP series were systematically exposed to COS-1 cells and uptake probed and confirmed using silver staining, fluorescent counterstaining, and dual mode fluorescence microscopy. We show that cellular uptake for the AuNPs in this series is directly dependent on the presence of CPP and that the ultimate intracellular destination is further determined by AuNP diameter. We also find that the CPP-conjugated AuNPs demonstrate minimal cytotoxicity over the concentration range required for efficient cellular uptake.

RESULTS

AuNP Synthesis and Surface Ligand Coverage. A detailed description of all synthetic and analytical procedures can be found in the Methods section below. For the purposes of this study, we synthesized a series of AuNPs where size increases were targeted to be approximately twice that of the smaller preceding particle. This resulted in a set of six increasingly larger AuNPs with diameters of 2.4, 5.5, 8.2, 16, 38, and 89 nm. The AuNPs are synthesized and stabilized in aqueous solution using thioctic acid−poly(ethylene glycol) (TA−PEG) ligands which provide several inherent benefits to the colloid. The multivalent binding interactions arising from the bidentate thiol motif imbue the ligand with a much higher affinity for the NP surface than similar monothiol molecules along with providing excellent long-term colloidal stability and resistance to salt and denaturing agents.[25] As the PEG's ethylene oxide repeats mediate solubility, rather than charge, such PEGylated AuNPs also demonstrate wide pH and buffer stability.[25,26] Lastly, the strongly neutral character of PEG molecules in general is widely exploited to prevent nonspecific adsorption and interactions such as opsonization in biological environments.[27,28]

As described in the Methods section, the smaller AuNPs (2.4, 5.5, 8.2, and 16 nm diameter) were prepared using a recently developed one-step aqueous-phase, room temperature synthetic method.[26] The larger-sized 38 and 89 nm AuNPs were synthesized using the same TA−PEG ligands with modifications of the procedure to a higher temperature and the serial addition of reagents. The TA−PEG ligands terminated in either an inert methoxy group (TA−PEG−OMe) or a carboxyl group (TA−PEG−COOH) (see Figure 1). Utilizing a mixture of these ligands during synthesis provides for mixed-surface NPs with the carboxyl also functioning as the site for further carbodiimide chemistry-based modification. Previous work had estimated the thiol coverage of divalent TA−PEG on the surface of these types of AuNP at ∼12% for 10−15 nm diameter AuNPs.[29] The number of ligands is half the thiol coverage given the bidentate dithiol headgroup. The dithiol also results in lower overall thiol coverage compared to monothiol ligands as it is believed to have a relatively large footprint of ∼1.2 nm^2 on the AuNP surface.[29] Using the method described in the Supporting Information, we estimate the number of ligands on the surface of the TA−PEG functionalized AuNPs to be ∼12 (2.4 nm), 73 (5.5 nm), 170 (8.2 nm), 660 (16 nm), 3800 (38 nm) and 21000 (89 nm) (see Table 1)

Characterization of AuNPs: UV−Visible Spectroscopy, Transmission Electron Microscopy, and Dynamic Light Scattering. Following synthesis, the PEG−functionalized AuNPs were subjected to stability tests in various buffer conditions including high concentrations of NaCl, a wide range of pH, and high dithiothreitol (DTT) concentrations, as described.[26] Similar to the previous results, the AuNP−TA−PEG complexes were found to be remarkably stable (data not shown), a result we ascribe to the combination of high colloidal stability imparted by the PEG component and the strong anchoring capacity of the bidentate thiol (TA) portion of the ligands.[25,26,29,30]

The colloidal AuNPs next underwent extensive photophysical characterization to help define the material size and associated properties. UV−vis spectroscopy examined the surface plasmon resonance band (SPB) of each material, see Figure 2a. Because of their small size, the 2.4 nm AuNPs did not exhibit a distinct SPB, only a broad shoulder was observed around 517 nm that resulted in a brown colored dispersion (Figure 2b).[8] The remaining 5.5−89 nm diameter AuNPs exhibited characteristic SPBs that both shifted to longer wavelengths and became more intense with increasing size (Figure 2a). Concomitant with the increases in size and SPB, the solutions had colors that ranged from wine-red to a metallic-golden magenta (Figure 2b). Concentrations of the AuNPs as synthesized and initially utilized here (working stock concentrations)

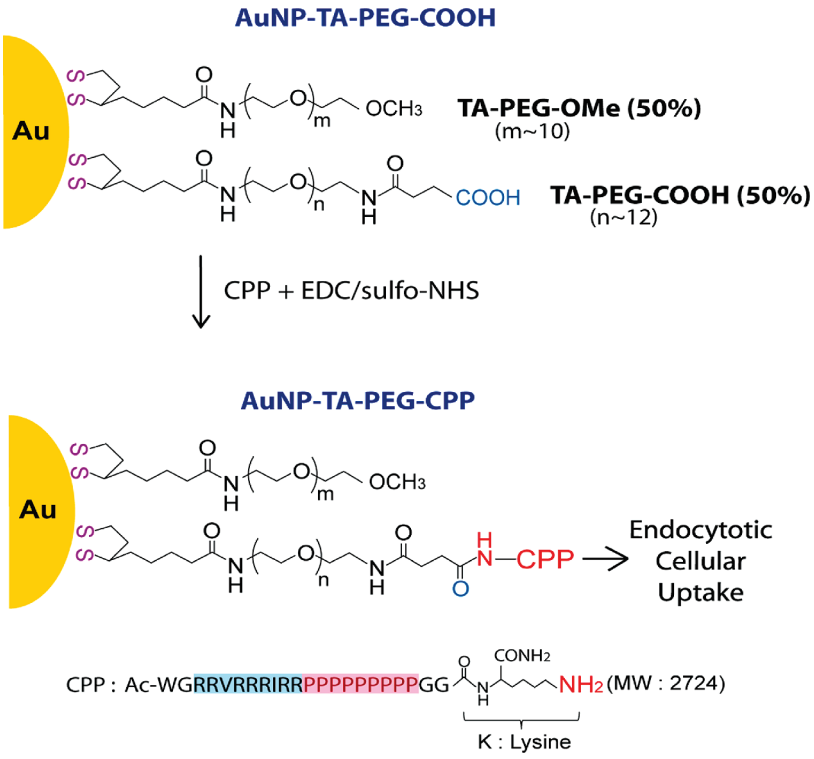

Figure 1. Schematic diagram of AuNP−TA−PEG−COOH (mixed surface of 50% of TA−PEG−COOH and 50% of TA−PEG−OMe) and AuNP−TA−PEG−CPP. Within the CPP sequence: Ac is an acetyl group blocking the N-terminus and $-CONH_2$ is an amide blocking the C-terminus. The unique primary amine on the lysine residue is highlighted by drawing out this residue, which acts as the target site for the EDC chemistry. The polyarginine CPP portion and the polyproline linker are highlighted in blue and red, respectively.

TABLE 1. Selected Gold Nanoparticle Characteristics and Estimates of Surface Ligand Coverage

Size (nm)	[Au][a] (μM)	D_H[b] (nm)	ε[c] (M^{-1} cm^{-1})	[AuNP] (nM)[d]	N_{Au}[e] Au atoms/NP	$N_{s\text{-}Au}$[e] surface Au atoms/NP	Estimated ligand/NP[f]	CPP/NP[g] reacted
2.4	285		8.1×10^5	670	430	210	12	30
5.5	285	8.9 ± 2.1	9.7×10^6	56	5100	1200	73	180
8.2	285	19 ± 4.7	5.6×10^7	17	17000	2800	170	400
16	285	28 ± 6.0	3.6×10^8	2.3	130000	11000	660	1600
38	285	75 ± 33.4	7.9×10^9	0.17	1700000	63000	3800	9000
89	285	122 ± 49.8	1.3×10^{11}	0.013	22000000	350000	21000	50000

[a] Total gold atom concentration used for AuNP synthesis. [b] Average hydrodynamic diameter intensity profiles determined with DLS. [c] Extinction coefficient calculated from TEM size and UV absorbance at 520 nm and number of Au per NP assuming 100% reaction yield. Note: The as-prepared AuNP colloids do not show the two distinct peaks at 220 and 290 nm for the pure aurate solutions, confirming that there is no more $AuCl_4$ present. [d] Concentration of AuNPs calculated from extinction coefficient and UV absorbance at 520 nm. [e] Estimated number of total Au atom per AuNP (N_{Au}) and number of surface Au atom per AuNP ($N_{s\text{-}Au}$) as described in the Supporting Information. [f] Estimated ligand number per AuNP based on ~12% NP surface thiol coverage as described in Supporting Information. [g] Ratio of CPP to AuNP during CPP conjugation reactions utilized a ~2.5-fold excess of CPP over carboxylated ligands present.

were estimated to be 670 nM (2.4 nm), 56 nM (5.5 nm), 17 nM (8.2 nm), 2.3 nM (16 nm), 0.17 nM (38 nm), and 0.013 nM (89 nm); these are the same values summarized in Table 1. For subsequent modification and cellular delivery, samples underwent concentration. AuNP physical size was measured using high resolution transmission electron microscopy (HR-TEM), see Figure 2c. The representative HR-TEM micrographs confirmed that the AuNPs have highly faceted nanocrystalline structures as expected. Analysis of the resultant images show that the NPs have, on average, a ~13.5% polydispersity in their individual size ranges with the 16 nm NPs displaying the smallest deviation at ~12% while the largest 89 nm particles varied by ~16%. These values are comparable to the range displayed by smaller thiol-stabilized 1−5 nm AuNPs synthesized using Brust's method.[8]

The hydrodynamic diameter of the AuNPs was further examined using dynamic light scattering (DLS), see Figure 2d. The extreme sensitivity of the scattered signal to changes in the radius (R) of the scattering objects (scattered intensity $\propto R^6$), enables DLS to detect even small fractions of aggregate build-up in NP dispersions. This is important, as AuNPs

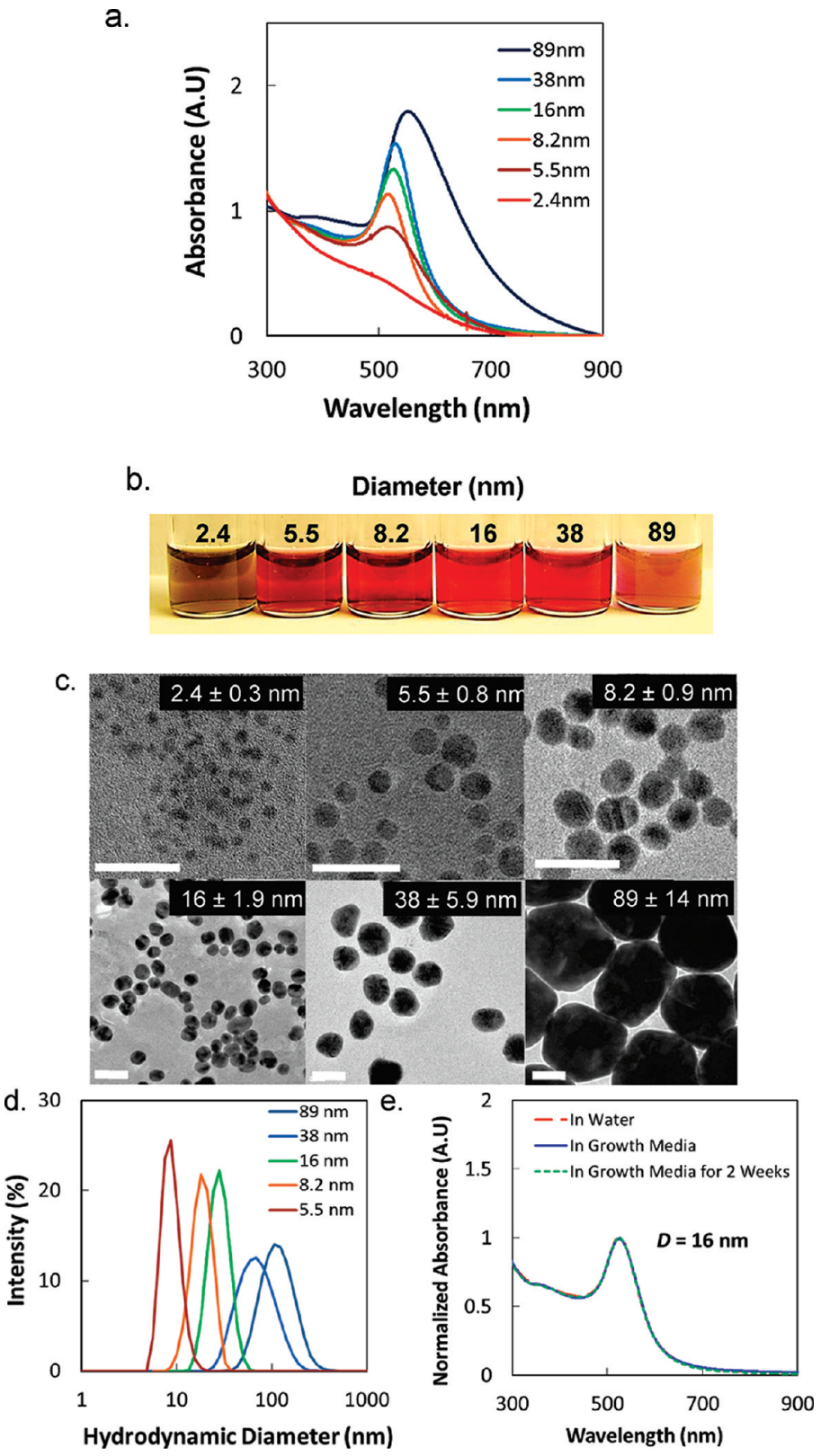

Figure 2. (a) Normalized UV–vis absorption spectra of AuNPs with different sizes. (b) Photographs of the colloidal AuNPs with different diameters (2.4–89 nm). Concentration of AuNPs: 670 nM (2.4 nm), 56 nM (5.5 nm), 17 nM (8.2 nm), 2.3 nM (16 nm), 0.17 nM (38 nm), 0.013 nM (89 nm). (c) TEM images of AuNPs. Average size and standard deviation are reported for each sample. Scale bars are 20 nm (top) and 40 nm (bottom). (d) The intensity plot of hydrodynamic diameter, of the AuNP series as determined using DLS. The averaged hydrodynamic diameters in intensity profile, D_H, were 8.9 ± 2.1, 19 ± 4.7, 28 ± 6.0, 75 ± 33.4, and 122 ± 49.8 nm for the 5.5–89 nm AuNPs, respectively (see also Table 1). (e) Absorption spectra of 16 nm diameter AuNP–TA–PEG–COOH (50% TA–PEG–COOH) in water (broken red line), in 50% growth media (blue solid line), and in the same 50% growth media after 2 weeks (green dashed line).

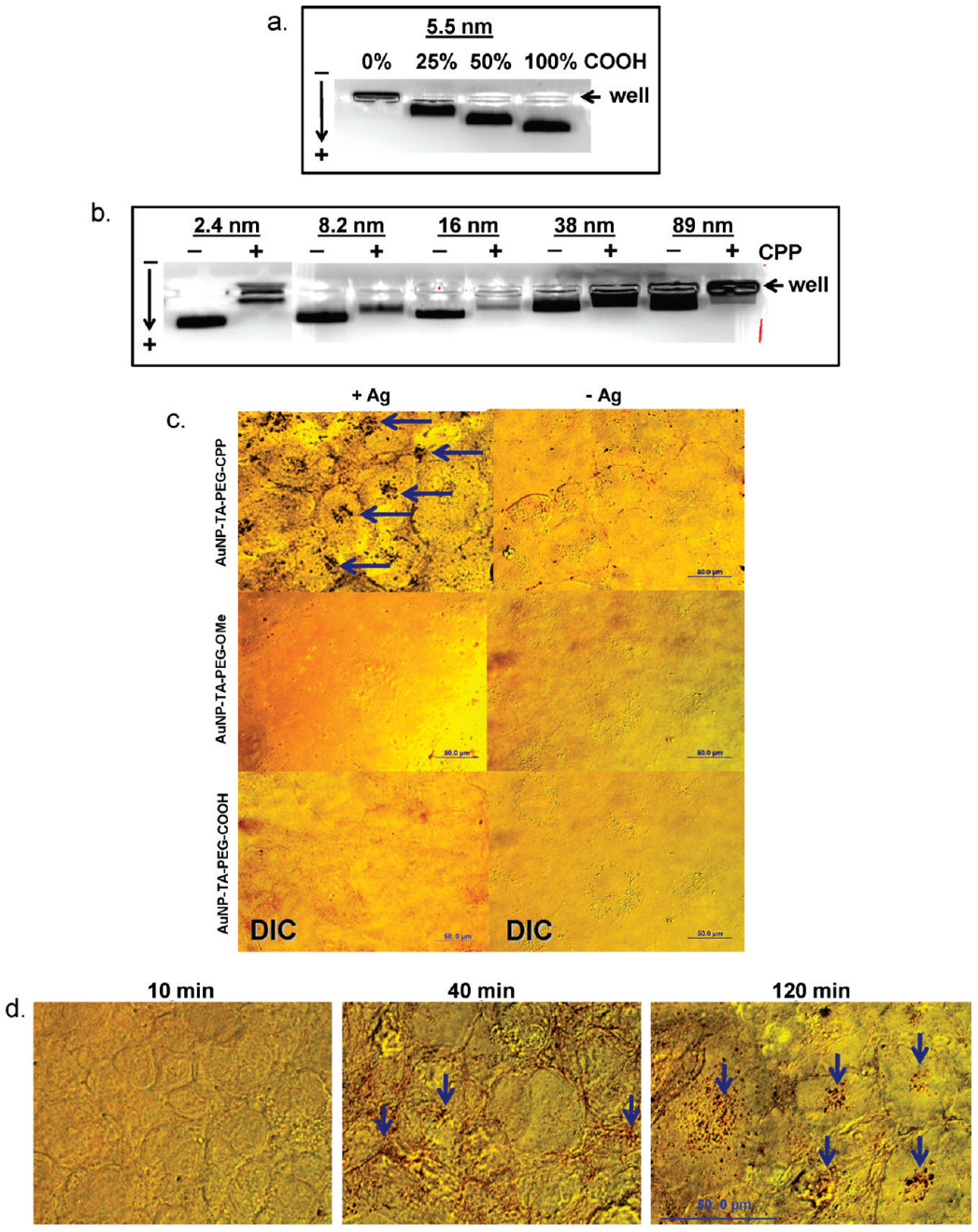

Figure 3. (a) Agarose gel electrophoretic separation of 5.5 nm AuNPs differently functionalized with increasing percentages of TA–PEG–COOH versus TA–PEG–OMe (0, 25, 50, 100%). (b) Agarose gel separation of various sized AuNP–TA–PEG–COOH (100% COOH for 2.4 nm and 50% COOH for 8.2, 16, 38, 89 nm AuNPs) before and after CPP conjugation. Samples in panels a and b consist of concentrated AuNP that is illuminated with indirect lighting (no silver staining was used in the gels). (c) DIC images of 8.2 nm diameter AuNPs either with (+Ag) or without silver-staining (−Ag). Samples consist of cells exposed to different materials as indicated and include AuNP–TA–PEG–CPP (top), AuNP–TA–PEG–OMe (middle), and AuNP–TA–PEG–COOH (bottom); 100 nM AuNP coincubated with cells for 3 h. (d) DIC images of 2.4 nm diameter AuNP–TA–PEG–CPP (125 nM) exposed to cells for the indicated time periods and then silver stained as described. The arrow highlights stained AuNP accumulation over time.

surface-stabilized with other ligands including sodium citrate and monothiol-appended-PEG frequently aggregate into larger-sized materials without precipitation.[26] Hydrodynamic measurement of the nanocrystals also takes into account subtle interactions between the solvent and surface-bound ligands, including ligand sizes and charges which yield larger hydrodynamic sizes than the core sizes measured by TEM. Results from DLS show the hydrodynamic sizes, given as the averaged size in intensity profile or D_H, to be 8.9 ± 2.1, 19 ± 4.7, 28 ± 6.0, 75 ± 33.4 and 122 ± 49.8 nm for the 5.5 to 89 nm NPs, respectively, see Table 1. These values are larger than the core sizes of the NP series from the TEM data, given the presence of the lengthy

PEG molecules on their surfaces and solvation effect. The PEG moieties are assumed to have a persistence length of around 2.5−3 nm in an energy minimized conformation (data not shown). The native 2.4 nm AuNPs did not undergo DLS analysis as their small size is below instrumental resolution. We were, however, able to measure the D_H of the 2.4 nm AuNP−TA−PEG−CPP conjugates, which helped confirm chemical conjugation (see following and Supporting Information). Gratifyingly, the DLS measurements confirmed that there was no visible aggregation within the AuNP solutions.

To further confirm stability and resistance to nonspecific adsorption in the same environment that the AuNPs would experience when exposed to cells, we monitored absorbance changes of AuNP−TA−PEG samples (16 nm diameter at ∼3 nM concentration, 50% TA−PEG−COOH) in concentrated 50% growth media (1 mL) over a 2 week period at room temperature. This high concentration of media was utilized to represent an environment that is more extreme than that in which the cells are manipulated and should force any potential interactions to occur. The representative results for the 16 nm sample presented in Figure 2e confirm no overt adsorption of materials over this time period. Similar results were collected for all the other particle sizes (data not shown). Adsorption of proteins and other materials to the NPs, (bio)etching of their surfaces, agglomeration, or similar undesired changes would all manifest in changes to the absorption spectra (for an example of such effects see Figure 4A in ref 31). Recent evidence suggests that such processes are also detrimental to cellular uptake.[16]

Covalent Modification of AuNPs with Cell Penetrating Peptide. To facilitate cellular uptake of the AuNP series, we utilized a CPP displaying multiple arginine residues. This positively charged motif is derived from the human immunodeficiency virus (HIV) transcriptional activator protein (Tat) and has been shown to mediate the endocytic uptake of a number of different NPs into eukaryotic cells.[32−35] It is widely believed that the arginine's inherently strong positive charge complexes to the negatively charged heparan sulfate proteoglycan receptors present on cellular membranes which then undergo endocytosis. The CPP sequence utilized here (Ac-WGR$_2$VR$_3$IR$_2$P$_9$G$_2$K-CONH$_2$) incorporates several modifications to optimize its intended function (see Figure 1). The N-terminus is blocked with an acetyl group (Ac), allowing the lysine side chain to provide a unique primary amine as the target for covalent carbodiimide chemistry. The C-terminus is blocked with an amide group (CONH$_2$) to prevent undesired cross-linking during the same chemistry. The two glycine residues function as a flexible hinge, while the nine consecutive prolines (highlighted red Figure 1) serve to provide a rigid type II helical extension away from the NP surface which allows the arginines unhindered interactions with the cell surface receptors. The arginine residues are also interspersed with the placement of other residues (highlighted in blue in Figure 1) to allow more flexibility in their interactions with the cell surface. Lastly, the tryptophan is inserted as a chromophore "handle" to allow quantitation of peptide concentration from its absorbance.

Maintaining control over ratios of CPP coupled to each NP sample is, in turn, based upon exerting intimate control over the ratio of carboxyl ligand displayed on the AuNPs. We performed preliminary experiments on the AuNP samples to verify this control. During synthesis, the ratios of TA−PEG−OMe/TA−PEG−COOH ligand was increased in discrete increments such that the percentage of carboxyl was varied from 0 to 100%. The resulting AuNPs were then separated in agarose gels as described in the Methods section. The same-sized AuNP samples should migrate in a manner that reflects the different amounts of deprotonated carboxyl groups displayed on their surface. As can be seen from the representative data collected in Figure 3a, where 5.5 nm AuNPs with various levels of surface coverage were separated, the relative mobility in the electric field for each sample is dependent upon its net charge. NPs displaying ligands terminating in only methoxyl groups (0% COOH) did not migrate due to their overall neutral charge. Increasing percentages of carboxyl groups displayed on the NP surface resulted in proportionally faster rates of migration through the gel with the 100% carboxylated sample demonstrating the highest mobility. Similar results were collected from the other AuNP samples (data not shown) confirming that control can be exerted over the relative ratios of a particular ligand attached to the NP surface during synthesis.

For peptide modification, AuNP samples were synthesized to display TA−PEG−OMe/TA−PEG−COOH ligand ratios of 1:1. The only exception was the 2.4 nm AuNP, which were surface-functionalized with 100% TA−PEG−COOH due to the small number of ligands expected to be present on these materials. The TA−PEG−COOH ligand is also slightly longer than the methoxy (by two ethylene oxide repeats, see Figure 1) to help facilitate subsequent CPP interactions with cell surfaces. AuNPs were then conjugated to the CPP using *N*-ethyl-*N*′-(3-dimethylaminopropyl)carbodiimide hydrochloride (EDC) and *N*-hydroxysulfosuccinimide (sulfo-NHS)[36] to form an amide bond between the PEG ligand's carboxyl group and the CPP's unique lysine-amine as described in the Methods section. Peptide modification of the AuNPs was again confirmed by gel electrophoresis as shown in Figure 3b, which highlights representative data from some of the AuNP samples. As can be seen in the gels, AuNP−TA−PEG−COOH complexes migrated toward the positive electrode due to their net negative charges. Following peptide conjugation, the

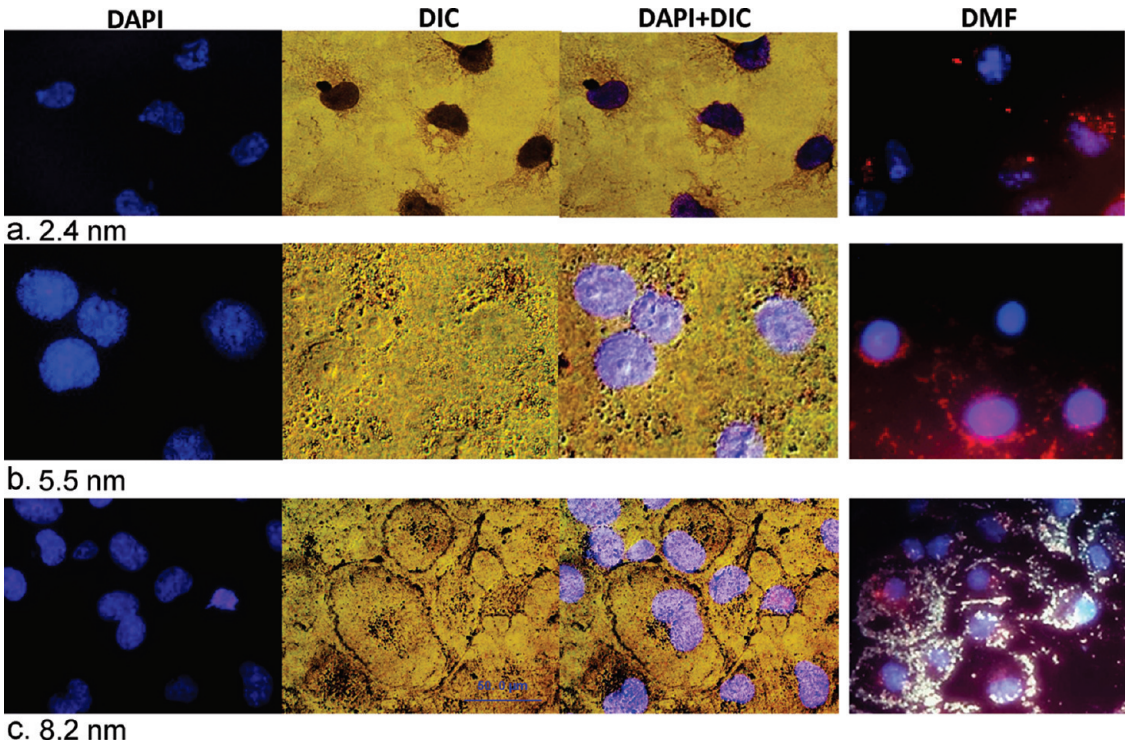

Figure 4. DAPI, DIC, DAPI-DIC merged, and DMF images following 3 h exposure and cellular uptake of 2.4 nm (125 nM), 5.5 nm (100 nM), and 8.2 nm (100 nM) AuNP−TA−PEG−CPP conjugates as described. The DAPI−DIC samples underwent silver enhancement prior to imaging while the DMF imaged samples did not. The DAPI, DIC, and DAPI−DIC merged images are of the same cells while the DMF images are of a different field of view. DMF conditions: triple pass filter for simultaneous DAPI, FITC, and Texas Red fluorescence and white light for the AuNP scattering of AuNPs (magnification 100×). The red fluorescence in the DMF image arises from Texas Red-labeled transferrin. Selected control images of blank samples are in the Supporting Information.

AuNP−TA−PEG−CPP complexes migrate more slowly than the unmodified NPs due to the combination of additional peptide mass and the arginine residue's opposite positive charge. Similar to the relative percentages of carboxyl ligand on the NPs, the maximum CPP coverage on the NPs should be around 50% of the total ligand coverage (see Table 1).

Zeta potentials for selected (5.5 and 8.2 nm AuNPs) AuNP−TA−PEG−COOH and AuNP−TA−PEG−CPP are provided in the Supporting Information. We do, however, qualify that the actual number of CPP attached/NP may be below these values due to reaction kinetics and possible steric hindrance from other CPP moieties already present on the NP surface.

Cellular Uptake of AuNP−TA−PEG−CPP Conjugates: Surface Chemistry and Delivery Time. For cellular delivery experiments, solutions of AuNPs were mixed with growth media as described in the Methods section and added to adherent monolayers of African green monkey kidney COS-1 cells seeded on fibronectin-coated eight-well chambered coverglass slides. This model cell line was utilized as it has previously undergone extensive utilization for testing the cellular delivery of many other NP materials including semiconductor quantum dots (QDs) along with those synthesized from iron oxide, glycol-chitosan, ORMOSIL, silica, polyethylenimine, polyallylamine, and more pertinently, a variety of differentially-sized or modified gold.[37−47] AuNP samples were incubated in duplicate wells for 2−3 h at 37 °C, washed with phosphate buffered saline (PBS) to remove unbound AuNPs, and fixed with 3.7% paraformaldehyde. Duplicate AuNP samples were visualized using either of two modalities. One sample underwent silver staining enhancement and differential interference contrast (DIC) imaging while the other sample was subjected to dual mode fluorescence (DMF) imaging. The latter technique uses dark-field-based illumination to measure simultaneous fluorescence (triple pass for DAPI, FITC, and Texas Red) along with nonfluorescent scattering signals from particulate matter that is ≥50 nm in diameter as described in the Methods section (see Supporting Figure S1 for an example image of 60 nm AuNPs scattering in solution). For most experiments, Texas-Red-labeled transferrin (TR-Tf) was added to the exposure media along with the AuNPs to label the endosomal pathway, and the nuclei were also counterstained with DAPI dye after fixation.

We first performed baseline experiments to determine the effect of AuNP surface chemistry on the specificity of cellular uptake in our system. For this, we incubated 8.2 nm-sized AuNP−TA−PEG−OMe,

AuNP−TA−PEG−COOH (50% TA−PEG−COOH) and AuNP−TA−PEG−CPP (CPP coupled with AuNP−TA−PEG−COOH) with cells under identical conditions at concentrations ranging from 20 to 250 nM. This size was chosen to represent an intermediary within the full range. Following DIC imaging of the silver-stained cell monolayer samples (Figure 3c), neither AuNP−TA−PEG−OMe nor AuNP−TA−PEG−COOH showed any significant binding to the cell membrane or delivery into the cell, confirming the inert nature of the PEG moiety. In contrast, cells incubated with AuNP−TA−PEG−CPP exhibited strong signals from the AuNPs on the cell membrane and within the cells in what appeared to be a central or perinuclear localization. These are visualized as the darker areas of staining where AuNPs are located as indicated by the blue arrows. We noted visible uptake for concentrations starting at 100−125 nM. This concentration range would be used for all subsequent experiments. Incubating cells with the same materials at 4 °C, where endocytosis is inhibited, did not result in uptake or subsequent staining (data not shown). These results strongly suggest that electrostatically neutral (methoxy) or negative (carboxyl) AuNP surfaces do not of themselves mediate cellular uptake and that the CPP is specifically required to facilitate endocytosis of the NP at these concentrations and cell exposure times.

A similar baseline experiment was also carried out to determine minimal delivery times. For this we selected 2.4 nm AuNP−TA−PEG−CPP conjugates, as we reasoned that the smallest NP should undergo the fastest rate of uptake barring any other circumstances, and should also require the most silver enhancement in order to be visualized. These were then exposed to replicate cells in the same manner for increasing time periods from 10 min to 2 h, fixed, and silver stained. As is shown in Figure 3d, the shortest time point of 10 min was insufficient for achieving visible levels of uptake at 125 nM concentration. At 40 min, significant amounts of material begin to appear accumulating at the cell membrane along with a small amount of intracellular staining. At 120 min, the majority of the AuNP conjugate yields an intracellular staining pattern which appears in the center of most cells. On the basis of these results, the following experiments were all performed using a 2−3 h incubation window.

Effect of AuNP Size on Intracellular Uptake and Localization. We next performed experiments where the series of increasingly larger AuNP−TA−PEG−CPP samples were systematically incubated with the cells in the same manner as described above. Following washing and fixation of the cells, delivery results were then probed with both silver staining/DIC imaging and DMF. Overall, the results from this system revealed clear differences in both delivery efficiency and intracellular fate that were directly dependent on AuNP size with materials localized to three distinct regions of the cells.

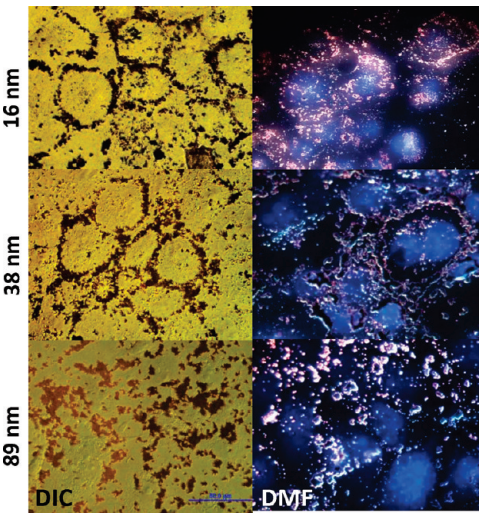

Figure 5. DIC and DMF images following cellular exposure of 16, 38, and 89 nm diameter AuNP−TA−PEG−CPP with (left, DIC) and without silver enhancing (right, DMF), respectively. DMF condition: triple pass for DAPI, FITC, and Texas Red and white light for the scattering of AuNPs (magnification 100×). Note: the reddish/white color in the DMF images for these images is not from Texas Red fluorescence but rather from strong scattering from the AuNPs.

Following the putative endosomal uptake, the smallest 2.4 nm particles appeared to be delivered primarily to the nucleus with some perinuclear staining also visible (see Figure 4a). The perinuclear staining was far less intense leading to the conclusion that most of the delivered material was nuclear localized. This was especially evident for the silver-stained samples, where a very high degree of co-localization between the stain and the fluorescent DAPI nuclear dye (blue) confirmed nuclear localization. Importantly, side-by-side staining in the exact same manner of control cells that were not exposed to the 2.4 nm AuNPs did not show any silver staining in the nuclei (data not shown). Additionally, exposing the same concentrations of control 2.4 nm AuNP−TA−PEG−COOH samples lacking CPP did not result in any intracellular uptake (Supporting Figure S2). DMF imaging of the same samples did not show any visible scattering from the AuNPs, as expected, given their extremely small size. Fluorescence from the TR-Tf (red) is also visible under DMF and highlights what appear to be perinuclear endosomes which correspond to the same cellular location as the small amount of perinuclear AuNP in the silver-stained images.

The 5.5 nm AuNP−TA−PEG−CPP conjugates demonstrated a far different intracellular staining pattern (see Figure 4b). In this case, silver enhancement highlighted a less intense staining pattern that appeared to be mostly perinuclear along with a small portion of material at the cellular periphery. DMF imaging again showed no scattering from the Au-NPs along with the presence of TR-Tf in cytoplasmic and perinuclear endosomes. We found that while DAPI remained

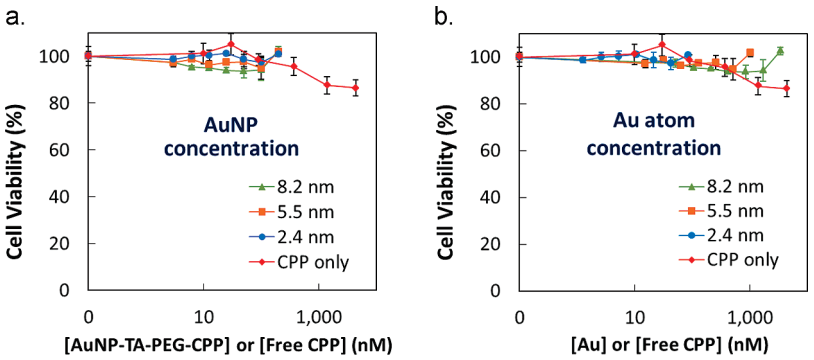

Figure 6. Cellular viability assays following delivery of the indicated AuNP–TA–PEG–CPP conjugates. (a) Percentage cellular viability *versus* exposure concentration of 2.4, 5.5, and 8 nm diameter AuNPs and free CPP. (b) Percentage cellular viability *versus* Au concentration corresponding to the Au atoms present in each increasingly larger AuNP along with free CPP.

fluorescent following silver enhancement, Texas Red emission was usually quite compromised. This made obtaining simultaneous TR-Tf fluorescence along with overlapping silver-stained AuNP images challenging. Nevertheless, in some cases we were able to obtain useful data. For example, see Supporting Figure S3 which confirms that the 5.5 nm AuNPs are indeed co-localization with TR-Tf in endosomes. Similar to the lack of uptake observed for unmodified AuNPs lacking CPP above, 5.5 nm-sized control unmodified citrate-stabilized AuNPs (obtained from Ted Pella, Inc.) also did not undergo uptake using the same experimental conditions and were washed away following incubation with the cells (Supporting Figure S4).

The CPP-functionalized 8.2 nm NPs demonstrated a somewhat similar delivery pattern that also displayed perinuclear and membranous staining (see Figure 4c). In contrast to the 5.5 nm conjugates, the majority of the material clearly remained at the membrane while a smaller portion appeared to be perinuclear. Owing to this sample's larger diameter, along with what we surmise to be a higher density of AuNP accumulated in the endosome or membrane, the scattering portion of the DMF imaging was far more informative. The corresponding DMF images collected from this delivery confirm that the majority of the NPs are indeed membranous, while a significantly smaller amount of material is perinuclear and demonstrates some co-localization with TR-Tf fluorescence. The ability to image intracellular 8.2 nm NP-complex scattering allowed us to again confirm CPP mediation of intracellular NP delivery, as exposing 8.2 nm AuNP–TA–PEG–COOH lacking CPP to the same cells resulted in no visible intracellular signal (Supporting Figures S2 and S5). Exposing 16, 38, and 89 nm diameter AuNP–TA–PEG–CPP conjugates to cells in the same manner did not result in any visible intracellular uptake (see Figure 5). Both DMF and DIC imaging of silver-stained cells exposed to the 16 and 38 nm materials demonstrate a very strong membranous accumulation of the NPs. In contrast, the 89 nm materials do not show such accumulation, but rather appear to have undergone a more general aggregation and precipitation across the field of view.

Toxicity of AuNP–TA–PEG–CPP Conjugates. Given the growing importance of NP toxicity issues,[1,2,23,48,49] we also assessed the cytotoxicity of the AuNP–TA–PEG–CPP assemblies. For this, we utilized a standard colorimetric cellular viability assay where MTT dye, 3-(4,5-dimethylthiazol-2-yl)-2,5-diphenyltetrazolium bromide, is converted to a blue formazan product whose absorbance can be measured (see Methods).[37,38,50] The assay essentially relies on the conversion of substrate to product by reducing mitochondrial enzymes within viable cells; the amount of color formation is directly proportional to the number of viable cells. We limited the testing to the 2.4, 5.5, and 8.2 nm diameter AuNPs as these demonstrated efficient uptake and intracellular delivery to different organelles in contrast to the larger sized particles which remained at the membrane. Increasing concentrations of the AuNP–TA–PEG–CPP assemblies were exposed to cells in replicate microtiter wells in the same manner. The cells were then washed and cultured for 3 days prior to the assay to assess the effects of endocytosed AuNPs on cellular turnover and viability.

Figure 6a shows the resulting cellular viability plotted against exposure concentration of AuNP–TA–PEG–CPP conjugates and free CPP (0–200 nM of AuNPs and 0–4.4 μM of free CPP) using a standard delivery time of 2 h. Minimal cytotoxicity was observed for the AuNP–TA–PEG–CPP conjugates even at the highest concentrations of 200 nM. The lowest cell viability values observed were 94% and 97% for the 8.2 and 2.4 nm conjugate materials, respectively, and are not significantly different from the unexposed control samples within assay error. Viability of cells exposed to free CPP dropped to 86% at the highest concentration of 4.4 μM tested here. Higher concentrations of free CPP were not warranted given that the AuNP–TA–PEG–CPP conjugate did not elicit any appreciable cytotoxicity. Figure 6b replots the data from Figure 6a in terms of total Au atomic dosage instead of discrete AuNP dosage.

Beyond gross cytotoxicity, we were also interested in assessing the amount of endotoxin present in our

"as-prepared" AuNPs. These lipopolysaccharides are ubiquitous in the environment and originate from the outer membrane of Gram-negative bacteria. More pertinently, they can trigger inflammatory responses in both cells and mammals.[51] Contamination of NPs with endotoxin during manufacture and handling of NPs prior to use is of high current concern given the wide projected applications of these materials in nanomedicine.[48,49] Although no regulations have been finalized for endotoxin levels in NP materials ultimately intended for medical applications *per se*, the allowable limits for medical devices in contact with blood is 20 endotoxin units (EU) per device (or 0.5 EU/ml × 40 mL = 20 EU/device).[48,49,52] As the model cell-line utilized here is not part of the immune system, we did not examine inflammatory responses, but rather focused on using traditional Limulus Amebocyte Lysate (LAL) assays, including gel clot- and kinetic chromogenic-based procedures, to quantify the endotoxin levels present in samples of the native PEG–modified AuNPs prior to CPP modification.

Preliminary screening of the 5.5 nm diameter AuNP stock prepared samples selected for testing by gel clot assay were positive and subsequent kinetic chromogenic assays determined that endotoxin was present at ~9.5 EU/mL (see Supporting Information). We followed this up by investigating whether the endotoxin concentration could be reduced by prior filtering of the sample. Samples were passed through 100 kDa molecular weight cutoff centrifuge filters which were effective at reducing the endotoxin to 1.6 EU/mL, a 6-fold reduction although still slightly above our nominally allowable limit of 0.5 EU/mL. We also tried combining filtering with a chromatography step using a polymyxin B column which selectively binds and removes endotoxin. This, however, resulted in a significant reduction in the final AuNP concentration and was not further pursued. Overall, we were gratified to find that the endotoxin concentrations in our samples, which were prepared without endotoxin-free water and in a normal lab environment rather than a clean facility, were relatively low and could be further reduced just by simple filtration. Clearly, further stringency during synthesis can reduce these values to negligible levels as needed.

DISCUSSION AND CONCLUSIONS

In this report, we use PEG–dithiolane ligands to synthesize a series of 6 AuNPs with different diameters that roughly double in size from 2.4 to 89 nm. We demonstrate that the presence of CPP displayed on the AuNP surface is the specific factor that mediates endocytosis and subsequent uptake under our specific cellular delivery conditions. More importantly, cellular uptake and final intracellular localization of the CPP-conjugated AuNPs was completely dependent on particle size. Concomitant cytotoxicity assays showed no adverse affects on cellular viability along with the presence of a small amount of endotoxin. Their small sizes, lack of fluorescence, and strong fluorescent quenching properties have made intracellular tracking of AuNPs challenging. To overcome this, we utilize a combination of silver staining/DIC imaging, fluorescent counterstaining, and DMF to follow NP fate in cells. Each of these procedures comes with its own set of benefits and potential problems. Although quite easy to implement, silver staining for example, can be compromised by overdevelopment and the need to judiciously discriminate between high background and real results. Fluorescence from counter-labeling of intracellular compartments can be easily quenched, especially by the nearby presence of larger AuNPs. DMF cannot readily image smaller particles *in situ* and strong scattering from larger NPs can interfere with other fluorescence that may be present. We, however, found the combination of all three imaging modalities to be complementary. DMF data matched well with the silver staining/DIC and was able to provide simultaneous data (*i.e.*, DAPI fluorescence and scattering; Figures 4 and 5) without requiring signal enhancement or switching between different filter cubes.

The smallest 2.4 nm particles appeared to be targeted to the nucleus with almost all the endocytosed material filling this organelle in the 2–3 h exposure period. This result has three important and related implications; the 2.4 nm AuNP–TA–PEG–CPP complexes: (i) most likely undergo endocytosis and subsequently escape the endolysosomal system; (ii) are recognized by nuclear pore proteins and undergo facilitated transport into the nucleus, (iii) and this all takes place in a short exposure time-period. The ability of the 2.4 nm AuNP–TA–PEG–CPP assemblies to initially escape the endosomes and access the cytoplasm is perplexing. There are reports of HIV-1 Tat protein-based CPPs facilitating endosomal escape and subsequent localization to the cytoplasm and/or nucleus of diverse cargo materials including fluorophores/dyes, nucleic acids, proteins, and even QDs.[16,33,37,53,54] It is important to note that this particular Tat-mediated endosomal escape mechanism remains controversial.[34,35] Moreover, our previous work with CPP-mediated delivery of somewhat larger semiconductor QDs did not yield any endosomal escape even when switching from negatively charged to neutral surface ligands.[30,37,38]

Nuclear uptake of cytosolic materials ranging from proteins to NPs usually requires the presence of nuclear localization signal (NLS) peptides. These were originally identified from the Simian virus 40 (SV40) large T-antigen core sequence PKKKRKV.[55,56] Most NLS derivatives are commonly based around a consensus of either one or multiple short sequences of positively charged lysine or arginine residues. Comparison to our

CPP shows an area of high homology around the reversed PRRIRRRV sequence with an identical predicted charge of ~5 at the slightly acidic cytosolic pH of 6.5−7.0 (www.scripps.edu/cgi-bin/cdputnam/protcalc3). Our CPP also displays the requisite multiple short sequences of positively charged arginine residues. This leads us to postulate that once the 2.4 nm AuNP−peptide conjugates are cytoplasmic, the surface-displayed CPP are recognized by the nuclear pore complex and taken into the nucleus. The size of the central pore in the complex has been estimated at ~44 nm.[57] Seminal work by Kann showed that they could bind and actively transport 26 nm diameter AuNPs coated with nuclear cargo-receptor complexes (bringing the diameter closer to 40 nm) into the nucleus using an *in vitro* recapitulated system.[58] Clearly, 2.4 nm AuNPs conjugated with an NLS-like peptide on their surfaces and displaying a hydrodynamic radius of 9.4 ± 1.5 nm in intensity profile and 8.4 ± 1.5 nm in number profile (Supporting Figure S6) should not represent a challenge for the nuclear pore complex system. This, combined with a much higher predicted avidity from multiply displayed peptides on the NP surface,[59] may explain the almost total nuclear uptake of this material in such a short time period. There are corroborating *in vitro* reports of different-sized AuNPs undergoing endocytosis and specific delivery to the nucleus in cells. Similar to our results, de la Fuente and Berry conjugated CPP to 2.8 nm Au-tiopronin NPs and demonstrated nuclear delivery in a telomerase-immortalized primary human fibroblast cell line.[60] Tkachenko showed that 20 nm AuNPs indirectly complexed to a SV40 NLS or other adenoviral peptides underwent endocytosis and nuclear delivery in a hepatocellular carcinoma HepG2 cell line.[19] Similarly, NLS conjugated 20−50 nm Au-nanorods achieved both cytoplasmic and nuclear delivery in a HaCaT human keratinocyte and HSC 3 human oral squamous cell carcinoma line.[17]

In contrast to nuclear localization, the intermediary sized 5.5/8.2 nm AuNPs underwent endocytic uptake but remained sequestered within the endolysomal system showing a strong perinuclear presence in conjunction with some material being retained at the membrane. Small differences were observed in the relative ratios of membranous *versus* perinuclear material delivered for each size although the reasons behind these subtle changes are unclear. These results are consistent to further work from Tkachenko who conjugated the protein transduction domain (PTD) of the HIV Tat protein to 20 nm AuNPs and monitored delivery in HepG2, HeLa human cervical epithelium, and 3T3/NIH murine fibroblastoma cells.[24] Their results again suggested endocytic uptake and perinuclear, but not nuclear, localization in the 3T3/NIH or HepG2 cells with the Tat-PTD. In contrast, labeling the same AuNPs with NLS or an integrin-binding domain showed nuclear uptake in HeLa and HepG2 cell lines. These mixed results serve to highlight the complexities present in these systems where merely switching between peptides or cell lines can yield an almost diametrically opposite outcome. Importantly, the authors posit that the AuNP−peptide conjugate must escape endosomal sequestration *before* undergoing nuclear uptake regardless of circumstance. Brust provided evidence supporting this by modifying 16 nm AuNPs with NLS in liposomes to circumvent initial endocytosis.[16] It is possible that given their smaller size, the 5.5/8.2 nm AuNP−TA−PEG−CPP conjugates would also undergo nuclear uptake if they accessed the cytoplasm. In conjunction with the 2.4 nm NP data above, this suggests that endosomal escape itself may have some dependency on size and peptide type. Overall, endocytic uptake along with perinuclear localization is perhaps the most common result reported for delivery of a wide size-range of AuNPs conjugates, and indeed other NP materials, to different cell lines.[1−4,8−11,16,22−24]

The failure of the 16 and 38 nm diameter AuNPs to demonstrate endocytic uptake within our experimental system is in direct contrast to other reports. Just using a criteria of diameter, endocytosis and cellular uptake have been reported for AuNP sizes of 13 nm,[18] 14 up to 100 nm NPs,[32] 15 up to 55 nm,[11] 1 up to 200 nm,[23] 16 nm,[16] 20 nm,[24] 45 nm,[61] and 70 nm.[62] Although many more examples exist, this approach does not account for any other variables (*i.e.*, ligand type, CPP presence, delivery time, *etc.*) which may be equally important to the outcome. However, the fact that these NP-conjugates appeared to concentrate at the cell membrane suggests that some initial CPP−membrane interactions did indeed take place. We, however, were unable to determine if these NPs were able to penetrate and cross the membrane in early endosomes or just remained at the periphery after washing out the free AuNPs. Extended incubation times (>3 h) can force NP uptake into cells; however, our focus was on size differences while minimizing all other variables. There may indeed have been some very low level of uptake for the larger 16 and 38 nm diameter particles, but this would be beyond the detection limits of the imaging techniques as applied here.

In terms of toxicity, we found no significant changes in cellular viability after cells were exposed to the 2.4−8.2 nm diameter AuNP−TA−PEG−CPP complexes. We ascribe this result to three related reasons: (i) the intrinsic chemistry of AuNPs, (ii) the stable, inert, and nonfouling nature of the surface PEG ligands, and (iii) the delivery regime utilized. Gold colloids are already a well-established pharmaceutical agent,[4] and we surmise that the current NP formulations are quite stable intracellularly over the 3-day culture time examined. Second, similar to their use in pharmaceutical

formulations and on myriad other biosurfaces, the PEG layer surrounding the NPs function as a potent and neutral antifouling agent preventing nonspecific adsorption and charge-driven interactions.[27,28] This was amply demonstrated by the unmodified nature of the AuNPs after exposure to growth media for 2 weeks (Figure 2e) and the complete lack of cellular binding noted for control AuNPs lacking CPP (Supporting Figures S2, and S5). The dithiol anchoring group attaching the PEG to the NP may also contribute to the lack of toxicity. Such bidentate interactions are far more stable than monothiol ligands which experience a high dynamic off-rate that destabilizes the colloid in biologically relevant reducing environments.[25,26,63] Lastly, we purposely selected delivery times and concentrations that would minimize the amount of AuNP conjugate to which the cell is exposed, while still allowing us to monitor uptake. Use of the same short or "acute" exposure times along with minimizing dosage when exposing cells to CPP-modified QDs were similarly found to significantly mitigate cytotoxicity.[37,38] These results contrast with many other reports of altered cellular viability in different configurations and indeed even these discrepancies are quite often also remarked upon in the literature.[1,20,22,23,64]

The growing importance of endotoxin contamination in NP materials, especially during synthesis, led us to examine its presence in our samples. Rather than gross cytotoxicity or loss of cellular viability, their ability to stimulate inflammatory responses or trigger other innate processes is the principal concern. This was eloquently demonstrated by Vallhov who showed that 12−51 ng of LPS/mL endotoxin contamination in 7 nm AuNP samples (also synthesized by a reduction chemistry) was the cause of cytokine upregulation and induction of maturation observed in exposed immature dendritic cells.[49] More pertinently, reducing endotoxin concentrations to below acceptable limits resulted in only a minor up-regulation of cytokines. We found a small amount of endotoxin present in our test samples which could be significantly reduced with filtration. Our current research is focused on achieving further reductions by synthesizing similar NP samples using endotoxin free reagents and a "clean" environment. Indeed, some preliminary synthesis using these criteria yielded materials with low endotoxin levels (data not shown).

Overall, this study demonstrated differential uptake kinetics and cellular targeting specificity for a designer-size series of PEGylated AuNP−CPP conjugates under stringent synthetic and delivery conditions in a model cell line. This suggests the potential for controlling cellular uptake and specific delivery of biologically active cargos to subcellular targets just by altering the size of the central AuNP nanoplatform. In conjunction with many other reports, these data also confirm that changing even one variable (*i.e.* size or CPP presence) can induce a very different outcome for NP materials exposed to cells. Here we are able to evaluate how the complex interplay between CPP presence, PEG presence, and NP size can alter intracellular fate. We recognize that many more variables (*i.e.*, different cell lines, exposure times, surface ligands, delivery peptides, *etc.*) than can be listed here must be still explored. This again reinforces the need for a systematic and exhaustive analysis of all relevant parameters.[20] As this challenge may be too large for one individual group to undertake, it is possible that continuing and cumulative reports from across this growing research field can strive to accomplish the same goal.

MATERIALS AND METHODS

Chemicals. *N*-Ethyl-*N*′-(3-dimethylaminopropyl)carbodiimide hydrochloride (EDC) and *N*-hydroxysulfosuccinimide (sulfo-NHS) were purchased from Pierce Biotechnology (Rockford, IL) and used as received. Agarose (low EEO) was purchased from Fisher Scientific. All the other chemicals (including solvents) were purchased from Sigma Aldrich or Acros Organics and used as received.

Dithiolane PEG Ligands. Poly(ethylene glycol)-modified thioctic acid ligands terminating in a methoxy (TA−PEG−OMe, average molecular weight of PEG ≈ 550, ethylene oxide repeat units, $m \approx 10$) or a carboxyl group (TA−PEG−COOH, averaged molecular weight of PEG ≈ 600, ethylene oxide repeat units, $n \approx 12$) were synthesized, purified, and characterized following the procedures detailed in refs 25, 30, 65, and 66 (see Figure 1 for the relevant structures.)

Synthesis of AuNPs (2.4−16 nm). This procedure is described in detail in ref 26. Briefly, in a typical reaction the following conditions were used to prepare the AuNPs: 156 μL (7.92×10^{-6} mol) of 50.8 mM tetrachloroauric (III) acid ($HAuCl_4 \cdot 3H_2O$) stock solution and the desired molar concentration of TA−PEG550−OMe were dissolved in 25 mL of deionized water; the mixture was then stirred at room temperature for 1 h; the stock solution of $HAuCl_4 \cdot 3H_2O$ was prepared by mixing 100 mg (2.54×10^{-4} mol) of $AuCl_4$ in 5 mL of H_2O. Then, 72 μL (6.3×10^{-5} mol) of 880 mM sodium borohydride ($NaBH_4$) stock solution in deionized water was added (in aliquots of 18 μL) over 30 min with vigorous stirring. To prepare different size nanoparticles, we fixed the molar concentration of $HAuCl_4$ and varied the amount of the ligands used. Ratios of 3:1, 100:1, 300:1 and 3000:1 of Au/ligand were used for 2.4, 5.5, 8.2, and 16 nm AuNPs, respectively, during the growth of the NPs. Following addition of the reducing agent the color of the reaction mixture immediately changed to brown (2.4 nm) or red (5.5, 8.2 nm). The mixture was then left stirring for at least 3 h as it gradually progressed to its final appearance (when the absorption spectrum reached saturation). For extra passivation and to allow later functionalization, TA−PEG550−OMe, TA−PEG600−COOH, or a mixture of TA−PEG550−OMe/TA−PEG600−COOH (final ratio of Au/ligand = 1:1) and 18 μL (1.6×10^{-5} mol) of 880 mM of $NaBH_4$ were further added to the AuNPs solution, and the mixture was left stirring for an additional 3 h. The dispersion was then purified from free ligands by three cycles of centrifugation using a membrane filtration device (100 K molecular weight cut-off, Millipore Corporation). AuNP dispersions were characterized using UV−vis spectroscopy, TEM, and DLS as described below.

Synthesis of AuNPs (38−89 nm). This procedure is a modification of ref 26. Briefly, 50 μL (50×10^{-6} mol) of 1 M citric acid

stock solution were dissolved in 50 mL of deionized water refluxing on a heating mantle and the mixture was stirred. 25 or 50 μL (2.5 or 5 $\times$ 10^{-6} mol) of 100 mM $HAuCl_4 \bullet 3H_2O$ stock solution and 2 or 4 μL (2.7 or 5.3 $\times$ 10^{-9} mol) of 1.33 mM TA–PEG550-OMe stock solution were injected into the reaction mixture while stirring. After approximately one minute following this injection, the color of the reaction solution changed from violet to pink. At this point, the next injection was performed. Following 3 to 6 further additions/injections, the heating mantle was removed and the reaction mixture was stirred for an additional 3 h as it gradually progressed to its final appearance, confirmed by the stabilization of the absorption spectrum. For extra passivation and to allow later functionalization, either pure TA–PEG550-OMe or a mixture of TA–PEG550-OMe/TA–PEG600-COOH (final ratio of Au:ligand =1:1) was added to the AuNPs solution and the mixture was left stirring for an additional 3 h. Final AuNP dispersions were purified and characterized as above.

UV–vis Spectroscopy and Transmission Electron Microscopy. Electronic absorption spectra were recorded using an HP 8453 diode array spectrophotometer (Agilent Technologies, Santa Clara, CA). The spectra were collected using quartz cuvettes (Spectro Cells) with 0.5 or 1 cm optical path length. Structural characterization of the AuNPs was carried out using a JEOL 2200-FX analytical high-resolution transmission electron microscope with a 200 kV accelerating voltage. Samples for TEM were prepared by spreading a drop of the AuNPs dispersion onto the holey carbon film of a fine mesh Cu grid (400 mesh) and letting it dry. Individual particle sizes were measured using Olympus measureIT (www.soft-imaging.net); average sizes along with standard deviations were extracted from the analysis of at least 100 nanoparticles.

Dynamic Light Scattering. DLS measurements were carried out using a CGS-3 goniometer system equipped with a HeNe laser illumination at 633 nm and a single-photon counting avalanche photodiode for signal detection (Malvern Instruments, Southcorough, MA). The autocorrelation function was performed by an ALV-5000/EPP photon correlator (ALV, Langen, Germany) and analyzed using Dispersion Technology Software (DTS) (Malvern Instruments). All AuNPs solutions were filtered through 0.45 μm syringe filters (Millipore Corporation) prior to DLS measurements. Sample temperature was maintained at 20 °C. For each sample, the autocorrelation function was the average of three runs of 10 s each and then repeated at different scattering angles (within 70° and 140°). CONTIN analysis was then used to extract intensity, number, and volume *versus* hydrodynamic size profiles for the dispersions studied.[67]

Gel Electrophoresis. Gel electrophoresis separation was conducted with AuNPs functionalized with 100% TA–PEG–OMe or a mixture of TA–PEG–OMe/TA–PEG–COOH. AuNPs were run on a 1% agarose gel buffered with Tris borate EDTA buffer (TBE, 100 mM Tris, 83 mM boric acid, 1 mM EDTA, pH 8.3). Samples were prepared in a 10% glycerol TBE loading buffer prior to loading. Separation voltages of 7–8 V/cm were used and images were captured using the white light mode of a Kodak Gel Logic 2200 Imaging System.

Preparation of AuNP–TA–PEG–Cell-Penetrating Peptide Conjugates. Carboxylated AuNPs (AuNP–TA–PEG–COOH) were covalently coupled to CPP at CPP/surface ligand ratios of 2.5:1. The excess CPP/AuNP ratios used in the coupling reactions were 30:1 (2.4 nm), 180:1 (5.5 nm), 400:1 (8.2 nm), 1600:1 (16 nm), 9000:1 (38 nm), 50000:1 (89 nm). Assuming our estimates of AuNP ligand density are correct and the reactions achieve stoichiometric labeling, the maximum amount of CPP (or ligand) per AuNP would be slightly less than half the excess reaction values (see also Table 1). Following synthesis, AuNPs were first concentrated up to 10-fold by using membrane filtration (5–100 K MW cutoff). Then 150 mM EDC and 7.5 mM sulfo-NHS (final concentrations), were reacted with the concentrated AuNPs and CPP in a 1 mL total reaction volume using phosphate buffered saline (PBS, 137 mM NaCl, 10 mM phosphate, 3 mM KCl, pH 7.4) for 2 h at room temperature. AuNP–TA–PEG–CPP conjugates were purified with a PD-10 desalting column (GE Healthcare, Piscataway NJ) using PBS as the eluting buffer and concentrated by membrane filtration (5–100 K MW cutoff) to concentrations of 0.4 nM (for 89 nm AuNPs) to 20 μM (for 2.4 nm AuNPs). AuNP–TA–PEG–CPP assemblies were stored at 4 °C until used.

Cell Culture and Delivery of AuNP–TA–PEG–CPP Conjugates. African green monkey kidney cells, COS-1 (American Type Culture Collection/ATCC, Manassas, VA), were cultured in Dulbecco's Modified Eagle's Medium (DMEM, ATCC) supplemented with 1% (v/v) antibiotic/antimycotic and 10% (v/v) heat inactivated fetal bovine serum. Cells were cultured in T-25 flasks and incubated at 37 °C under 5% CO_2 atmosphere and subculture was performed every 3–4 days as described.[37,38] Prior to delivery, 2 $\times$ 10^4 cells were seeded into the wells of Lab-Tek 8-well chambered coverglass (Nalge Nunc) and grown in the same manner overnight. Estimated number of cells at time of Au delivery is ~2.8 $\times$ 10^4 based on a 48 h COS-1 doubling time (ATCC). AuNPs were diluted into DMEM at concentrations ranging from 0.2 nM up to 250 nM and incubated with the cells for 2–3 h at 37 °C in a humidified incubator under 5% CO_2 atmosphere. Endosomes were counterstained by inclusion of 30 μg/mL Texas-Red-labeled-transferrin (Invitrogen) was also added in some cases during NP delivery.[37,38] Cells were then washed with PBS and fixed with 3.7% paraformaldehyde, and the AuNPs were stained for ~5 min using a silver staining enhancer kit (Sigma-Aldrich).[68,69] Nuclei were counterstained with 2 μg/mL of DAPI in PBS.

Imaging. The slides prepared above were imaged using an Olympus BX41 microscope (Olympus America Inc., Center Valley, PA) adapted with a CytoViva advanced illumination system equipped with a Dual Mode Fluorescence (DMF) module and an Exfo X-cite 120Q fluorescent light source (CytoViva, Inc. Auburn, AL). The CytoViva DMF system uses darkfield-based illumination and allows the simultaneous fluorescent and non-fluorescent imaging of the sample. The DMF module contains DAPI, FITC, and Texas Red filter sets as well as a triple pass (TP) option which allows the user to image all three simultaneously. In addition to fluorescence excitation, white light from the source can be simultaneously bled into the illumination to allow direct observation of the nonfluorescent portions of the sample along with Mie scattering from materials such as the AuNPs used here. The high optical resolution of the Cytoviva technology dramatically improves contrast and signal-to-noise ratios over conventional microscopes, leading to more detailed images. Sample slides with a coverslip attached were assembled above the condenser using type A immersion oil, and once aligned the slides were imaged using the TP filter with and without white light, using either the 40$\times$ or 100$\times$ objective lens. Images were captured using a QImaging Retiga-2000R charge coupled device (CCD) camera mounted on the microscope controlled using QCapture software (Surrey, Canada). In most cases a minimum of three images per sample were recorded. Alternatively epifluorescence image collection was carried out using an Olympus IX-71 total internal reflection fluorescence microscope equipped with a 60$\times$ or 100$\times$ oil immersion lens where samples were illuminated with a Xe lamp for UV excitation or a visible/bright light source. Differential interference contrast images (DIC) were collected using the bright light source.

Cytotoxicity of AuNP–TA–PEG–CPP Conjugates. Cellular viability was assessed by measuring cellular proliferation using the CellTiter 96 Cell Proliferation Assay (Promega, Madison, WI).[37,38,50] The assay is based upon the enzymatic conversion of a 3-(4,5-dimethylthiazol-2-yl)-2,5-diphenyltetrazolium bromide (MTT) substrate to a formazan product by viable cells at the assay end point. Cells were plated at a density of 5 $\times$ 10^3/well in a 96-well plate. Estimated number of cells at time of Au delivery is ~7 $\times$ 10^3 based on a 48 h COS-1 doubling time (ATCC). After 24 h, the cells were exposed to different concentrations of AuNP–TA–PEG–CPP (3.0, 6.2, 12.5, 25, 50, 100, and 200 nM) or free CPP (10, 30, 90, 370, 1400, 4400 nM) and incubated for 2 h in tissue culture media. Replicate wells containing cells and cell culture medium only (no AuNPs) were set as the negative control, while wells containing cell culture medium alone (no cells and no AuNPs) were used as the blank control. After removing AuNP–TA–PEG–CPP or CPP, cells were washed with PBS and then grown in fresh tissue culture media for 72 h. Then

20 μL of MTT reagent was added directly to the tissue culture media. After 4 h of coincubation, the absorbance of the plate was read at 562 nm. As the assay is an enzymatic assay, the absorbance was read once color formation had reached a suitable optical density (determined empirically using standards in all assays). The percent viability of the experimental wells was determined as the percent color formation relative to control wells (no AuNP–TA–PEG–CPP or free CPP). The relative viability (%) of the cells exposed to AuNP–TA–PEG–CPP or CPP was compared to that of the original negative control.

Gel Clot and Kinetic Chromogenic LAL Endotoxin Assay. Two traditional limulus amebocyte lysate (LAL) tests were used in this study to characterize the endotoxin levels in the as-prepared AuNPs.[52,70] Both the gel clot and the kinetic chromogenic assays were purchased from Associates of Cape Cod (East Falmouth, MA) and performed per the manufacturer instructions. The assays were calibrated using standard controls (certified endotoxin free) with known amounts of control standard endotoxin (CSE from *E. coli*) both obtained from Associates of Cape Cod).

Acknowledgment. The authors acknowledge NRL, the NRL NSI, ONR, DTRA/ARO, DARPA, and FDA Contract HHSF223200610765P for financial support. J.B.B.-C. acknowledges a Marie Curie IOF.

FDA Disclaimer. The mention of commercial products, their sources, or their use in connection with material reported herein is not to be construed as either an actual or implied endorsement of such products by the Department of Health and Human Services.

Supporting Information Available: Additional experimental details, a description of how the NP surface ligand coverage was estimated, determination of selected zeta potentials, supporting microscopic imaging data, and endotoxin testing procedures. This material is available free of charge *via* the Internet at http://pubs.acs.org.

REFERENCES AND NOTES

1. Alkilany, A. M.; Murphy, C. J. Toxicity and Cellular Uptake of Gold Nanoparticles: What We Have Learned So Far? *J. Nanopart. Res.* **2010**, *12*, 2313–2333.
2. Boisselier, E.; Astruc, D. Gold Nanoparticles in Nanomedicine: Preparations, Imaging, Diagnostics, Therapies and Toxicity. *Chem. Soc. Rev.* **2009**, *38*, 1759–1782.
3. Ghosh, P.; Han, G.; De, M.; Kim, C. K.; Rotello, V. M. Gold Nanoparticles in Delivery Applications. *Adv. Drug Delivery Rev.* **2008**, *60*, 1307–1315.
4. Giljohann, D. A.; Seferos, D. S.; Daniel, W. L.; Massich, M. D.; Patel, P. C.; Mirkin, C. A. Gold Nanoparticles for Biology and Medicine. *Angew. Chem., Int. Ed.* **2010**, *49*, 3280–3294.
5. Sau, T. K.; Rogach, A. L.; Jackel, F.; Klar, T. A.; Feldmann, J. Properties and Applications of Colloidal Nonspherical Noble Metal Nanoparticles. *Adv. Mater.* **2010**, *22*, 1805–1825.
6. Au, L.; Zheng, D. S.; Zhou, F.; Li, Z. Y.; Li, X. D.; Xia, Y. N. A Quantitative Study on the Photothermal Effect of Immuno Gold Nanocages Targeted to Breast Cancer Cells. *ACS Nano* **2008**, *2*, 1645–1652.
7. Qian, X. M.; Nie, S. M. Single-Molecule and Single-Nanoparticle SERS: From Fundamental Mechanisms to Biomedical Applications. *Chem. Soc. Rev.* **2008**, *37*, 912–920.
8. Daniel, M. C.; Astruc, D. Gold Nanoparticles: Assembly, Supramolecular Chemistry, Quantum-Size-Related Properties, and Applications Toward Biology, Catalysis, and Nanotechnology. *Chem. Rev.* **2004**, *104*, 293–346.
9. Thurn, K. T.; Brown, E. M. B.; Wu, A.; Vogt, S.; Lai, B.; Maser, J. R.; Paunesku, T.; Woloschak, G. E. Nanoparticles for Applications in Cellular Imaging. *Nano. Res. Lett.* **2007**, *2*, 430–441.
10. Arvizo, R. R.; Miranda, O. R.; Thompson, M. A.; Pabelick, C. M.; Bhattacharya, R.; Robertson, J. D.; Rotello, V. M.; Prakash, Y. S.; Mukherjee, P. Effect of Nanoparticle Surface Charge at the Plasma Membrane and Beyond. *Nano Lett.* **2010**, *10*, 2543–2548.
11. Cho, E. C.; Au, L.; Zhang, Q.; Xio, Y. The Effects of Size, Shape, and Surface Functional Group of Gold Nanostructures on Their Adsorption and Internalization by Cells. *Small* **2010**, *6*, 517–522.
12. Hong, R.; Han, G.; Fernandez, J. M.; Kim, B. J.; Forbes, N. S.; Rotello, V. M. Glutathione-Mediated Delivery and Release Using Monolayer Protected Nanoparticle Carriers. *J. Am. Chem. Soc.* **2006**, *128*, 1078–1079.
13. Hutter, E.; Boridy, S.; Labrecque, S.; Lalancette-Hebert, M.; Kriz, J.; Winnik, F. M.; Maysinger, D. Microglial Response to Gold Nanoparticles. *ACS Nano* **2010**, *4*, 2595–2606.
14. Jiang, W.; Kim, B. Y. S.; Rutka, J. T.; Chan, W. C. W. Nanoparticle-Mediated Cellular Response is Size-Dependent. *Nat. Nanotechnol.* **2008**, *3*, 145–150.
15. Loo, C.; Lowery, A.; Halas, N. J.; West, J.; Drezek, R. Immunotargeted Nanoshells for Integrated Cancer Imaging and Therapy. *Nano Lett.* **2005**, *5*, 709–711.
16. Nativo, P.; Prior, I. A.; Brust, M. Uptake and Intracellular Fate of Surface-Modified Gold Nanoparticles. *ACS Nano* **2008**, *2*, 1639–1644.
17. Oyelere, A. K.; Chen, P. C.; Huang, X. H.; El-Sayed, I. H.; El-Sayed, M. A. Peptide-Conjugated Gold Nanorods for Nuclear Targeting. *Bioconjugate Chem.* **2007**, *18*, 1490–1497.
18. Patel, P. C.; Giljohann, D. A.; Seferos, D. S.; Mirkin, C. A. Peptide Antisense Nanoparticles. *Proc. Natl. Acad. Sci. U.S.A.* **2008**, *105*, 17222–17226.
19. Tkachenko, A. G.; Xie, H.; Coleman, D.; Glomm, W.; Ryan, J.; Anderson, M. F.; Franzen, S.; Feldheim, D. L. Multifunctional Gold Nanoparticle-Peptide Complexes for Nuclear Targeting. *J. Am. Chem. Soc.* **2003**, *125*, 4700–4701.
20. Verma, A.; Stellacci, F. Effect of Surface Properties on Nanoparticle-Cell Interactions. *Small* **2010**, *6*, 12–21.
21. Verma, A.; Uzun, O.; Hu, Y. H.; Hu, Y.; Han, H. S.; Watson, N.; Chen, S. L.; Irvine, D. J.; Stellacci, F. Surface-Structure-Regulated Cell-Membrane Penetration by Monolayer-Protected Nanoparticles. *Nat. Mater.* **2008**, *7*, 588–595.
22. Levy, R.; Shaheen, U.; Cesbron, Y.; See, V. Gold Nanoparticles Delivery in Mammalian Live Cells: A Critical Review. *Nano Rev.* **2010**, *1*, 4889.
23. Khlebtsov, N.; Dykman, L. Biodistribution and Toxicity of Engineered Gold Nanoparticles: A Review of *in Vitro* and *in Vivo* Studies. *Chem. Soc. Rev.* **2011**, *40*, 1647–1671.
24. Tkachenko, A. G.; Xie, H.; Liu, Y. L.; Coleman, D.; Ryan, J.; Glomm, W. R.; Shipton, M. K.; Franzen, S.; Feldheim, D. L. Cellular Trajectories of Peptide-Modified Gold Particle Complexes: Comparison of Nuclear Localization Signals and Peptide Transduction Domains. *Bioconjugate Chem.* **2004**, *15*, 482–490.
25. Mei, B. C.; Oh, E.; Susumu, K.; Farrell, D.; Mountziaris, T. J.; Mattoussi, H. Effects of Ligand Coordination Number and Surface Curvature on the Stability of Gold Nanoparticles in Aqueous Solutions. *Langmuir* **2009**, *25*, 10604–10611.
26. Oh, E.; Susumu, K.; Goswami, R.; Mattoussi, H. One-Phase Synthesis of Water-Soluble Gold Nanoparticles with Control over Size and Surface Functionalities. *Langmuir* **2010**, *26*, 7604–7613.
27. Mintzer, M. A.; Grinstaff, M. W. Biomedical Applications of Dendrimers: A Tutorial. *Chem. Soc. Rev.* **2010**, *40*, 173–190.
28. Ryan, S. M.; Mantovani, G.; Wang, X. X.; Haddleton, D. M.; Brayden, D. J. Advances in PEGylation of Important Biotech Molecules: Delivery Aspects. *Exp. Opin. Drug Delivery* **2008**, *5*, 371–383.
29. Oh, E.; Susumu, K.; Blanco-Canosa, J. B.; Medintz, I. L.; Dawson, P. E.; Mattoussi, H. Preparation of Stable Maleimide-Functionalized Au Nanoparticles and Their Use in Counting Surface Ligands. *Small* **2010**, *6*, 1273–1278.
30. Susumu, K.; Uyeda, H. T.; Medintz, I. L.; Pons, T.; Delehanty, J. B.; Mattoussi, H. Enhancing the Stability and Biological Functionalities of Quantum Dots *via* Compact Multifunctional Ligands. *J. Am. Chem. Soc.* **2007**, *129*, 13987–13996.
31. Chithrani, B. D.; Ghazani, A. A.; Chan, W. C. W. Determining the Size and Shape Dependence of Gold Nanoparticle Uptake into Mammalian Cells. *Nano Lett.* **2006**, *6*, 662–668.

32. Vivès, E.; Schmidt, J.; Pèlegrin, A. Cell-Penetrating and Cell-Targeting Peptides in Drug Delivery. *B.B.A. Rev. Cancer* **2008**, *1786*, 126–138.
33. Delehanty, J. B.; Mattoussi, H.; Medintz, I. L. Delivering Quantum Dots into Cells: Strategies, Progress and Remaining Issues. *Anal. Bioanal. Chem.* **2009**, *393*, 1091–1105.
34. Delehanty, J. B.; Boeneman, K.; Bradburne, C. E.; Robertson, K.; Bongard, J. E.; Medintz, I. L. Peptides for Specific Intracellular Delivery and Targeting of Nanoparticles: Implications for Developing Nanoparticle-Mediated Drug Delivery. *Ther. Delivery* **2010**, *1*, 411–433.
35. Delehanty, J. B.; Boeneman, K.; Bradburne, C. E.; Robertson, K.; Medintz, I. L. Quantum Dots: A Powerful Tool for Understanding the Intricacies of Nanoparticle-Mediated Drug Delivery. *Exp. Opin. Drug Delivery* **2009**, *6*, 1091–1112.
36. Hermanson, G. T. *Bioconjugate Techniques,* 2nd ed.; Academic Press, Inc.: San Diego, CA, 2008.
37. Delehanty, J. B.; Bradburne, C. E.; Boeneman, K.; Susumu, K.; Farrell, D.; Mei, B. C.; Blanco-Canosa, J. B.; Dawson, G.; Dawson, P. E.; Mattoussi, H.; *et al*. Delivering Quantum Dot−Peptide Bioconjugates to the Cellular Cytosol: Escaping from the Endolysosomal System. *Integr. Biol.* **2010**, *2*, 265–277.
38. Delehanty, J. B.; Medintz, I. L.; Pons, T.; Brunel, F. M.; Dawson, P. E.; Mattoussi, H. Self-Assembled Quantum Dot−Peptide Bioconjugates for Selective Intracellular Delivery. *Bioconjugate Chem.* **2006**, *17*, 920–927.
39. Long, M. J. C.; Pan, Y.; Lin, H. C.; Hedstrom, L.; Xu, B. Cell Compatible Trimethoprim-Decorated Iron Oxide Nanoparticles Bind Dihydrofolate Reductase for Magnetically Modulating Focal Adhesion of Mammalian Cells. *J. Am. Chem. Soc.* **2011**, *133*, 10006–10009.
40. Yoo, H. S.; Lee, J. E.; Chung, H.; Kwon, I. C.; Jeong, S. Y. Self-Assembled Nanoparticles Containing Hydrophobically Modified Glycol Chitosan for Gene Delivery. *J. Controlled Release* **2005**, *103*, 235–243.
41. Chen, G.; Takezawa, M.; Kawazoe, N.; Tateishi, T. Preparation of Cationic Gold Nanoparticles for Gene Delivery. *Open Biotechnol. J.* **2008**, *2*, 152–156.
42. Roy, I.; Ohulchanskyy, T. Y.; Bharali, D. J.; Pudavar, H. E.; Mistretta, R. A.; Kaur, N.; Prasad, P. N. Optical Tracking of Organically Modified Silica Nanoparticles as DNA Carriers: A Nonviral, Nanomedicine Approach for Gene Delivery. *Proc. Natl. Acad. Sci. U.S.A.* **2005**, *102*, 279–284.
43. Nimesh, S.; Goyal, A.; Pawar, V.; Jayaraman, S.; Kumar, P.; Chandra, R.; Singh, Y.; Gupta, K. C. Polyethylenimine Nanoparticles as Efficient Transfecting Agents for Mammalian Cells. *J. Controlled Release* **2006**, *110*, 457–468.
44. Pathak, A.; Aggarwal, A.; Kurupati, R. K.; Patnaik, S.; Swami, A.; Singh, Y.; Kumar, P.; Vyas, S. P.; Gupta, K. C. Engineered Polyallylamine Nanoparticles for Efficient *in Vitro* Transfection. *Pharm. Res.* **2007**, *24*, 1427–1440.
45. Lewinski, N.; Colvin, V.; Drezek, R. Cytotoxicity of Nanoparticles. *Small* **2008**, *1*, 26–49.
46. Kim, S.; Ohulchanskyy, T. Y.; Baev, A.; Prasad, P. N. Synthesis and Nanoparticle Encapsulation of 3,5-Difuranylvinyl-boradiaza-*s*-indacenes for Near-Infrared Fluorescence Imaging. *J. Mater. Chem.* **2009**, *20*, 3181–3188.
47. Murphy, C. J.; Gole, A. M.; Stone, J. W.; Sisco, P. N.; Alkilany, A. M.; Goldsmith, E. C.; Baxter, S. C. Gold Nanoparticles in Biology: Beyond Toxicity to Cellular Imaging. *Acc. Chem. Res.* **2008**, *41*, 1721–1730.
48. Esch, R. K.; Han, L.; Foarde, K. K.; Ensor, D. S. Endotoxin Contamination of Engineered Nanoparticles. *Nanotoxicology* **2010**, *1*, 73–83.
49. Vallhov, H.; Qin, J.; Johansson, S. M.; Ahlorg, N.; Muhammed, M. A.; Scheynius, A.; Gabrielsson, S. The Importance of an Endotoxin-Free Environment During the Production of Nanoparticles Used in Medical Applications. *Nano Lett.* **2006**, *6*, 1382–1386.
50. Cory, A. H.; Owen, T. C.; Barltrop, J. A.; Cory, J. G. Use of an Aqueous Soluble Tetrazolium/Formazan Assay for Cell Growth Assays in Culture. *Cancer. Commun.* **1991**, *3*, 207–12.
51. Ianaro, A.; Tersigni, M.; D'Acquisto, F. New Insight in LPS Antagonist. *Mini-Rev. Med. Chem.* **2009**, *9*, 306–317.
52. Dobrovolskaia, M. A.; Neun, B. W.; Clogston, J. D.; Ding, H.; Ljubimova, J.; McNeil, S. E. Ambiguities in Applying Traditional Limulus Amebocyte Lysate Tests to Quantify Endotoxin in Nanoparticle Formulations. *Nanomedicine* **2010**, *5*, 555–562.
53. Melikov, K.; Chernomordik, L. Arginine-Rich Cell Penetrating Peptides: From Endosomal Uptake to Nuclear Delivery. *Cell. Mol. Life Sci.* **2005**, *62*, 2739–2749.
54. Zhao, M.; Weissleder, R. Intracellular Cargo Delivery Using Tat Peptide and Derivatives. *Med. Res. Rev.* **2004**, *24*, 1–12.
55. Dingwall, C.; Laskey, R. A. Nuclear Targeting Sequences−A Consensus. *Trends Biochem. Sci.* **1991**, *16*, 478–481.
56. Makkerh, J. P.; Dingwall, C.; Laskey, R. A. Comparative Mutagenesis of Nuclear Localization Signals Reveals the Importance of Neutral and Acidic Amino Acids. *Curr. Biol.* **1996**, *6*, 1025–1027.
57. Hinshaw, J. E.; Carragher, B. O.; Milligan, R. A. Architecture and Design of the Nuclear Pore Complex. *Cell* **1992**, *69*, 1133–1141.
58. Panté, N.; Kann, M. Nuclear Pore Complex Is Able To Transport Macromolecules with Diameters of ~39 nm. *Mol. Biol. Cell* **2002**, *13*, 425–434.
59. Mammen, M.; Choi, S. K.; Whitesides, G. M. Polyvalent Interactions in Biological Systems: Implications for Design and Use of Multivalent Ligands and Inhibitors. *Angew. Chem., Int. Ed.* **1998**, *37*, 2755–2794.
60. de la Fuente, J. M.; Berry, C. C. Tat Peptide as an Efficient Molecule To Translocate Gold Nanoparticles into the Cell Nucleus. *Bioconjugate Chem.* **2005**, *16*, 1176–1180.
61. Wang, S. H.; Lee, C. W.; Chiou, A.; Wei, P. K. Size-Dependent Endocytosis of Gold Nanoparticles Studied by Three-Dimensional Mapping of Plasmonic Scattering Images. *J. Nanobiotechnol.* **2010**, *8*, 33.
62. Petersen, S.; Barchanski, A.; Taylor, U.; Klein, S.; Rath, D.; Barcikowski, S. Penetratin-Conjugated Gold Nanoparticles—Design of Cell-Penetrating Nanomarkers by Femtosecond Laser Ablation. *J. Phys. Chem. C* **2011**, *115*, 5152–5159.
63. Liu, W. H.; Choi, H. S.; Zimmer, J. P.; Tanaka, E.; Frangioni, J. V.; Bawendi, M. Compact Cysteine-Coated CdSe(ZnCdS) Quantum Dots for *in Vivo* Applications. *J. Am. Chem. Soc.* **2007**, *129*, 14530–14531.
64. Schaeublin, N. M.; Braydich-Stolle, L. K.; Schrand, A. M.; Miller, J. M.; Hutchison, J.; Schlagera, J. J.; Hussain, S. M. Surface Charge of Gold Nanoparticles Mediates Mechanism of Toxicity. *Nanoscale* **2011**, *3*, 410–420.
65. Mei, B. C.; Susumu, K.; Medintz, I. L.; Delehanty, J. B.; Mountziaris, T. J.; Mattoussi, H. Modular Poly(ethylene glycol) Ligands for Biocompatible Semiconductor and Gold Nanocrystals with Extended pH and Ionic Stability. *J. Mater. Chem.* **2008**, *18*, 4949–4958.
66. Susumu, K.; Mei, B. C.; Mattoussi, H. Multifunctional Ligands Based on Dihydrolipoic Acid and Polyethylene Glycol to Promote Biocompatibility of Quantum Dots. *Nat. Protoc.* **2009**, *4*, 424–436.
67. Pons, T.; Uyeda, H. T.; Medintz, I. L.; Mattoussi, H. Hydrodynamic Dimensions, Electrophoretic Mobility and Stability of Hydrophilic Quantum Dots. *J. Phys. Chem. B* **2006**, *110*, 20308–20316.
68. Taton, T. V.; Mirkin, C. A.; Letsinger, R. L.; Scanometric, D. N. A. Array Detection with Nanoparticle Probes. *Science* **2000**, *289*, 1757–1760.
69. Teasdale, J.; Jackson, P.; Holgate, C. S.; Cowen, P. N. Identification of Estrogen Receptors in Cells of Paraffin-Processed Breast Cancers by IGSS. *Histochemistry* **1987**, *87*, 185–187.
70. Levin, J.; Bang, F. B. Clottable Protein in Limulus: Its Localization and Kinetics of Its Coagulation by Endotoxin. *Thromb. Diath. Haemorrh.* **1968**, *19*, 186–197.